PIER C

(Received 17 June 2024, Accepted 13 August 2024, Scheduled 26 August 2024)

Novel Compact UWB Antenna Design with Notch Filter Characteristics: Development and Performance Enhancement

Ujjval Dave[1, 2, *], Shahidmohammed Modasiya[2], Abhinav Dave[3], and Rahulkumar Patel[3]

[1] *Gujarat Technological University, Gujarat, India*
[2] *Electronics & Communication Engineering Department, Government Engineering College, Gandhinagar, Gujarat, India*
[3] *Electronics & Communication Engineering Department, Government Engineering College, Bharuch, Gujarat, India*

ABSTRACT: This paper introduces a novel compact microstrip-fed ultra-wideband (UWB) antenna, characterized by its unique square patch design and integrated parasitic circular patch for frequency band rejection. The antenna, fabricated on an FR4 substrate, exhibits dimensions of $0.17\lambda_g \times 0.17\lambda_g$, optimizing space without compromising performance. A significant innovation of this design is the incorporation of a parasitic circular patch with a carefully optimized radius of $0.02\times\lambda_g$ mm, achieving a remarkable return loss of -43 dB at 3.55 GHz, while frequencies ranging from 5.43 to 7.1 GHz exhibit significant notching. This feature effectively eliminates unwanted frequency bands, enhancing the antenna's application in UWB systems. Comprehensive analysis demonstrates that the antenna maintains an omnidirectional radiation pattern and achieves a desirable gain, making it highly compatible with a variety of UWB-enabled devices. The integration of the parasitic circular patch within the compact design not only improves the antenna's spectral purity but also contributes to its practical applicability in modern wireless communication systems. The findings underscore the potential of this antenna design in advancing UWB technology applications, offering a balance among compactness, efficiency, and performance.

1. INTRODUCTION

Ultra-wideband (UWB) technology [1–3], defined by its operation over a wide spectrum of frequencies typically ranging from 3.1 to 10.6 GHz, represents a significant advancement in wireless communication. Characterized by its high data transmission rates, minimal emission power, and cost-efficiency, UWB has emerged as a pivotal solution for numerous applications requiring rapid data exchange and low-power operation [4, 5]. The genesis of UWB can be traced back to military and radar applications, with its evolution marked by significant milestones that have expanded its utility into civilian domains such as asset tracking, through-wall imaging, and short-range communications. This broad-spectrum utilization enables UWB systems to achieve fine temporal resolution, making them exceptionally suited for applications demanding precise positioning and timing capabilities [6, 7].

The adoption of UWB technology has been further propelled by its integration into various commercial and industrial applications, ranging from wireless peripherals and home entertainment systems to automotive radar and smart home technologies [8, 9]. This diversification has been driven by UWB's inherent advantages, including its ability to coexist with existing narrowband and carrier-based systems without causing interference, courtesy of its low emission levels. Furthermore, the technology's resilience to multipath fading and penetration capabilities through obstacles has rendered it indispensable in complex environments, promoting seamless connectivity and enhanced user experiences.

Despite its vast potential and growing list of applications, the deployment of UWB technology faces challenges, particularly in the realm of antenna design and manufacturing. The need to mitigate interference from other bands, such as those used by WLAN (5.15–5.825 GHz) and WiMAX (5.25–5.85 GHz) systems, has necessitated the development of antennas with band-notched features [10–12]. Traditional approaches often resulted in complex structures that were not only difficult to manufacture but also costly. However, recent advancements have led to innovative solutions that simplify the antenna design, reducing manufacturing complexities and costs while maintaining performance efficacy. The evolution of manufacturing techniques, including printed monopole antennas with vertical coupling strips, signifies a notable shift towards more efficient, cost-effective, and compact designs, facilitating the broader adoption of UWB technology across various sectors. This paper delves into such advancements, highlighting the critical role of simplified yet effective antenna designs in overcoming manufacturing hurdles, thereby ushering in a new era of UWB application and development [13, 14].

2. DESIGN OF A SQUARE PATCH UWB ANTENNA WITH INTEGRATED PARASITIC CIRCULAR PATCH FOR ENHANCED FREQUENCY SELECTIVITY

The innovative design of the UWB antenna introduced in this work is predicated on a square patch geometry integrated with a parasitic circular patch, fabricated on a $0.01\lambda_g$ thick FR4 substrate. The substrate's choice is critical, characterized by its dielectric constant (ϵ_r) and loss tangent (δ), pa-

* Corresponding author: Ujjval Dave (ujjval21101986@gmail.com).

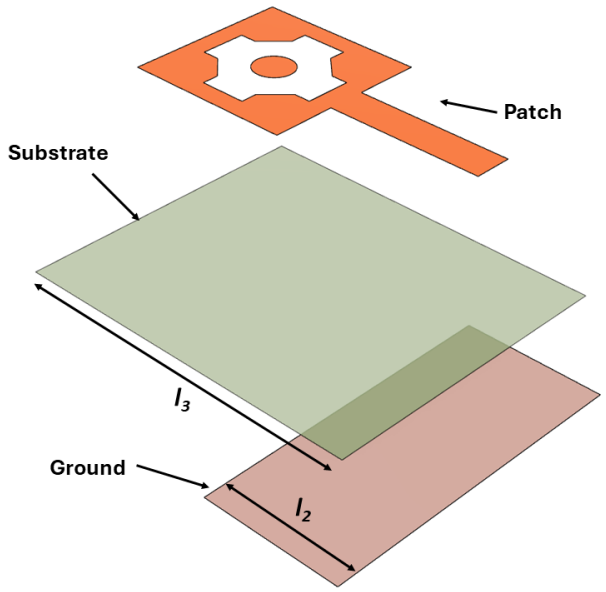

FIGURE 1. Schematic of the UWB antenna featuring an integrated parasitic circular patch for precision frequency control.

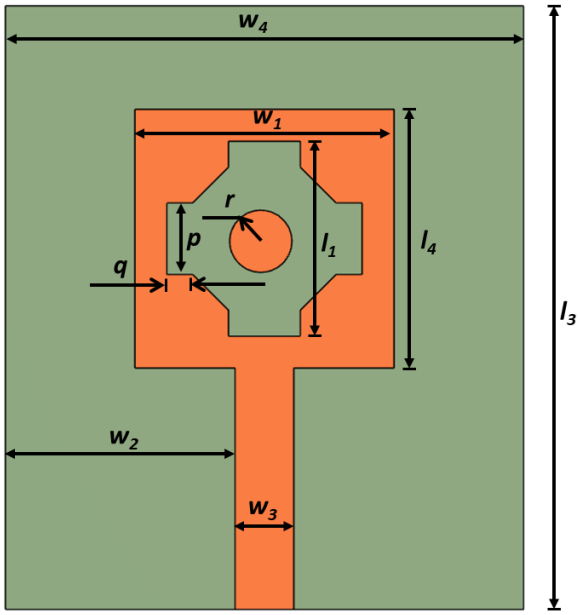

FIGURE 2. Detailed schematic of the UWB antenna featuring an integrated parasitic circular patch for precision frequency control.

rameters essential for determining the antenna's performance in UWB applications. This design, shown in Figures 1 and 2, leverages a 50 Ω microstrip line for feeding, with a width of $0.04\lambda_g$ mm, ensuring optimal impedance matching across the UWB spectrum. The antenna's dimensions are compact, measuring $0.17\lambda_g \times 0.17\lambda_g$, with a ground plane preciously selected to be $0.15\lambda_g$ mm in length and of adequate width to support the UWB operation while maintaining a minimal footprint. Dimensions of the proposed design are given in Table 1.

TABLE 1. Parameters and values.

Parameter	w_1	w_2	w_3	w_4
Value	$0.17\lambda_g$	$0.15\lambda_g$	$0.04\lambda_g$	$0.34\lambda_g$

Parameter	l_1	l_2	l_3	l_4
Value	$0.09\lambda_g$	$0.15\lambda_g$	$0.40\lambda_g$	$0.17\lambda_g$

Parameter	p	q	r
Value	$0.04\lambda_g$	$0.014\lambda_g$	$0.02\lambda_g$

Figure 1 illustrates a microstrip patch antenna design with a circular parasitic patch. The antenna consists of a copper radiating element (orange) on a dielectric substrate (green). The radiating element has a unique slotted geometry, resembling a square with four protruding arms, each with a circular notch cut out. This feature is not merely aesthetic but serves a pivotal role in the antenna's functionality. The patch introduces a mechanism for fine-tuning the S-parameters, particularly beneficial for mitigating interference and enhancing the selectivity of the antenna across its operational bandwidth. The design facilitates the adjustment of the patch's radius, offering a versatile tool for manipulating the antenna's resonant frequency and achieving desired rejection bands within the UWB range.

The rectangular patch serves as a fundamental shape for various types of microstrip antennas. Its resonant frequency can be expressed as [15]:

$$f_r = \frac{c_0}{2\left(L + 2\Delta W\right)\sqrt{\varepsilon_e(W)}} \tag{1}$$

where:

f_r : Resonant frequency of the rectangular patch antenna

c_0 : Speed of light in a vacuum

L : Effective length of the patch antenna

$\varepsilon_e(W)$: Effective dielectric constant

ΔW : Extension in length due to the fringing effect, dependent on the width W

Additionally, the radius r refers to the radius of the patch. Understanding f_r is essential for optimizing antenna performance, ensuring efficient signal transmission, and minimizing signal losses. This equation is crucial for determining the appropriate cable dimensions and operational frequency range.

The shape of the slot in the patch significantly impacts the antenna's impedance matching, bandwidth, and notching characteristics. In this design, a circular shape was selected due to its ability to provide a good balance among these parameters. The circular slot aids in achieving a low return loss at 3.55 GHz by effectively tuning the resonance frequency, thus improving the overall impedance matching of the antenna. The slot shape also affects the current distribution on the patch, which in turn influences the bandwidth. The circular slot design has demonstrated an appreciable bandwidth suitable for UWB applications. Additionally, the pronounced notching from 5.43 to 7.1 GHz is primarily due to the presence of the circular slot, which creates a band-stop filter effect. This notching is beneficial for avoiding

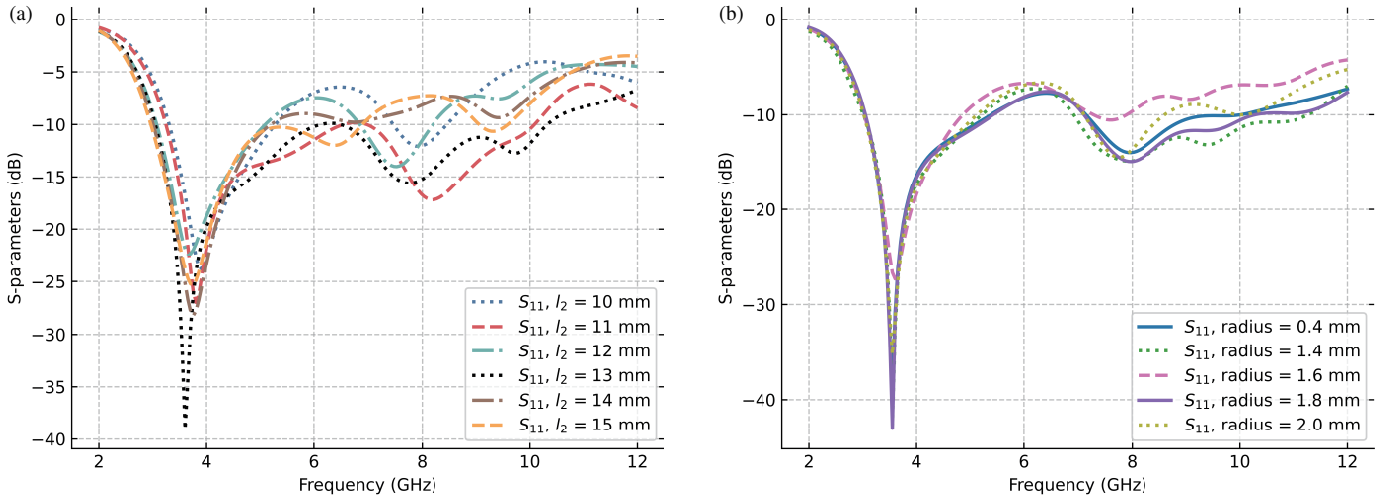

FIGURE 3. Findings: Variations in return loss across various design parameters for enhancing stopband performance. (a) Variation in base width of the patch. (b) Variation in parasitic circular patch element radius.

interference with other signals, such as those from WLAN and other communication systems.

Simulations with different slot shapes (rectangle, ellipse, and cross) indicated that the circular slot provided the best overall performance in terms of return loss, bandwidth, and notching characteristics. The circular slot resulted in a more uniform current distribution and fewer spurious resonances, which are advantageous for maintaining stable performance across the UWB range. The dimensions of the circular slot (radius and position) were optimized using advanced simulation software, with parametric studies determining the optimal values. Experimental validation showed that the measured results confirmed the simulated performance, thus validating the choice of the circular slot. The return loss and notching characteristics were consistent with design predictions.

Furthermore, the design's efficacy and the impact of the parasitic circular patch on the antenna's performance were validated through comprehensive simulation using the High Frequency Structure Simulator (HFSS) software. This involved an iterative process of adjusting design parameters, including the patch's radius r, to refine the antenna's impedance bandwidth and achieve optimal S-parameter profiles. The simulation results confirmed the antenna's ability to selectively filter out undesired frequencies while maintaining a broad operational bandwidth, a testament to the design's effectiveness.

The prototype's construction was guided by these optimized parameters, resulting in an antenna capable of superior performance in UWB applications. The integration of the parasitic circular patch within the square patch not only underscores the antenna's innovative design but also exemplifies a practical approach to achieving enhanced frequency selectivity and interference mitigation in compact UWB systems. This design strategy, supported by both theoretical and empirical analyses, paves the way for the development of highly efficient, tunable antennas suited for the ever-expanding sphere of UWB applications.

3. RESULTS AND DISCUSSION

An evaluation was conducted to assess the performance of the proposed UWB antenna design. Utilizing advanced simulation software, the antenna's characteristics were analyzed and compared with measured results. The dimensions of the parasitic circular patch and its base width were determined through iterative parameter adjustments to achieve optimal performance. Several design parameters were systematically varied and evaluated to ensure that the antenna produced the desired output characteristics. These variations, as illustrated in Figure 3(a) for base width (l_2) of the patch and Figure 3(b) for parasitic circular patch element radius, demonstrate their impact on key metrics such as return loss, crucial for enhancing stopband performance across different operational scenarios.

Utilizing HFSS, an in-depth exploration was conducted on the stopband characteristics across varying radius (r) of the parasitic circular patch. The simulation outcomes, depicted in Figure 3, reveal that the stopband frequency range can be adeptly tuned between 4.85 and 7.28 GHz.

Figure 4 presents a comprehensive depiction of the return losses across varying frequencies. The outcomes demonstrate a commendable level of agreement between the simulation predictions and the measurements. Notably, the measured impedance bandwidth, characterized by a 10 dB return loss, spans across the band, effectively excluding the frequency range of 5.43–7.10 GHz. This deliberate exclusion mitigates potential interference effects, enhancing the antenna's resilience in complex frequency environments. To go deeper into the band-notched feature, a thorough examination of the surface current distribution was performed at the frequency of 3.55 GHz for the antenna design.

The observed shift in the lower edge of the acclaimed notch frequency from 5.43 GHz in simulation to 5.9 GHz in measurement is likely attributed to a combination of factors inherent in the transition from theoretical modeling to physical realization. Parasitic effects, arising from the packaging, soldering, and lay-

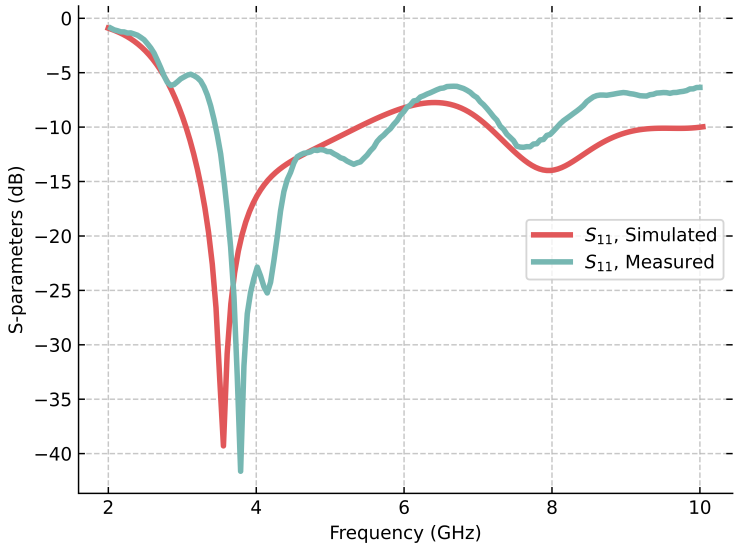

FIGURE 4. Analysis of return loss: Simulated & measured results of the antenna prototype.

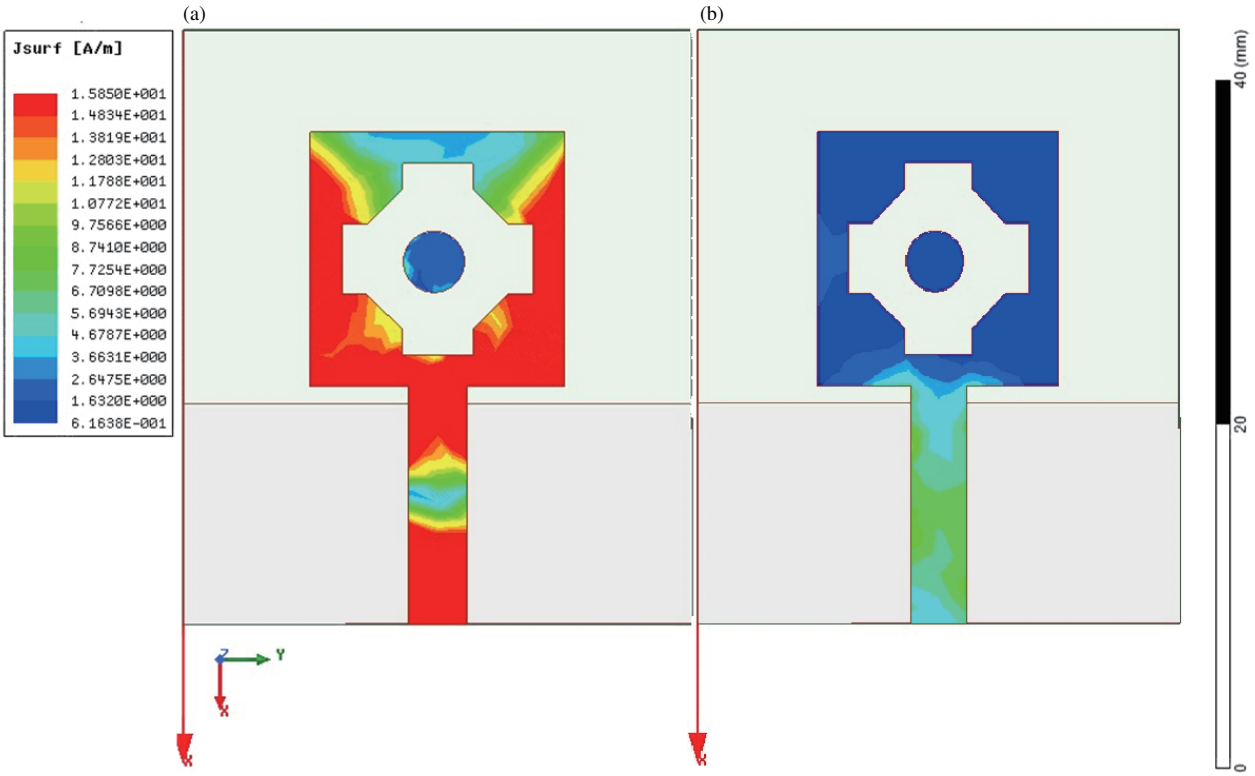

FIGURE 5. Comparison of surface current distributions (Jsurf) on the structure at (a) at frequency of 3.55 GHz (b) at frequency of 6.27 GHz.

out of the device, introduce additional capacitance and inductance not fully accounted for in the simulation. These parasitics can alter the resonant behavior and shift the notch frequency. Furthermore, slight deviations in the dielectric constant and loss tangent of the substrate material between the simulation and actual device can affect signal propagation and contribute to the frequency discrepancy. Fabrication tolerances, leading to variations in component dimensions, also play a role in modifying the effective capacitance and inductance, thus impacting the resonant frequency. While careful modeling and calibration procedures aim to minimize these discrepancies, the inherent complexities in translating simulations to physical devices often lead to observable shifts in critical parameters such as the notch frequency.

As illustrated in Figure 5, a discernible enhancement in resonance is observed surrounding the coupling strip compared to

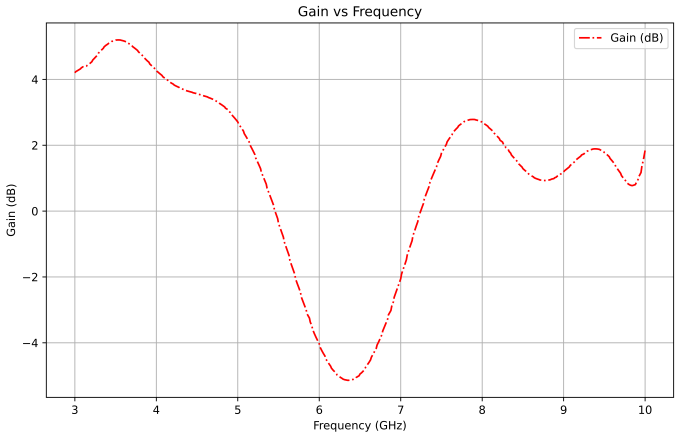

FIGURE 6. Gain versus frequency for the single element design.

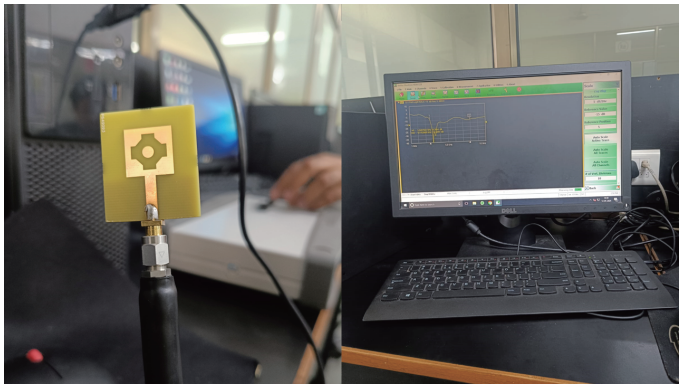

FIGURE 7. Anritsu MS46122B compact USB vector network analyzer: S-parameters measurement set-up.

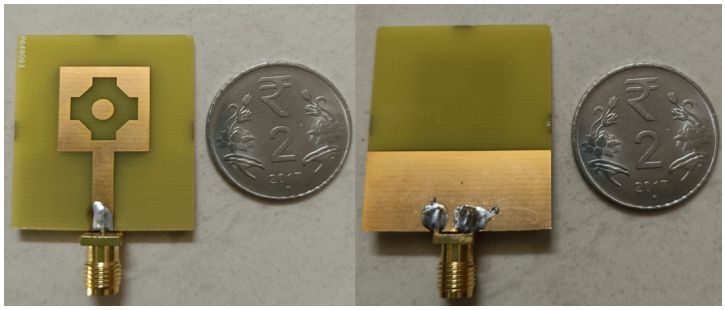

FIGURE 8. Fabricated proposed antenna prototype.

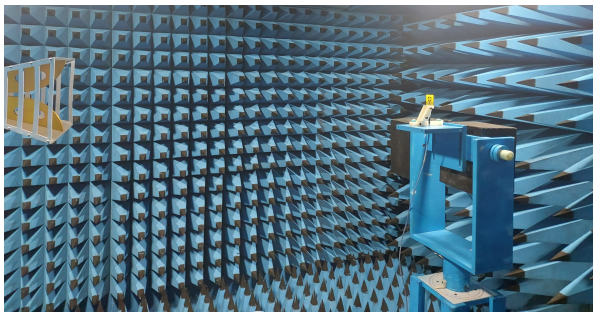

FIGURE 9. Radiation pattern measurement setup for proposed antenna prototype.

the conventional square slot patch configuration. This observation underscores the efficacy of our design in achieving robust frequency rejection characteristics. This direct visual comparison of the behavior at both frequencies highlights the distinct patterns associated with the resonance phenomenon, providing a clearer understanding of the surface current behavior.

As far as the effectiveness of the notch is concerned, we have conducted a thorough analysis of the realized gain within the stop band. Figure 6 demonstrates the gain versus frequency characteristics of our design. As shown, there is a significant reduction in gain within the 5.43–7.1 GHz stopband, indicating effective suppression of unwanted frequencies. This substantial drop in realized gain confirms the effectiveness of our notch, even with the S_{11} value being -7 dB.

The measurement setup for evaluating the proposed antenna prototype utilizes advanced instrumentation, including the Anritsu MS46122B Compact USB Vector Network Analyzer for precise S-parameters assessment as shown in Figure 7. Concurrently, the fabricated antenna prototype is visually represented in Figure 8, showcasing its structural details and compact form factor optimized for practical deployment in communication systems. The antenna's radiation pattern is also analyzed using dedicated measurement configurations as depicted in Figure 9, ensuring comprehensive characterization of its directional properties and spatial coverage capabilities. These setups are carefully calibrated to maintain measurement accuracy, crucial for validating the antenna's performance across specified frequency bands and operational scenarios.

Figure 10 presents the simulated and measured far-field radiation patterns in the E-plane and H-plane at a frequency of 3.55 GHz. The results depict nearly ideal omnidirectional patterns in the H-plane, suggesting strong consistency between simulation and measurement. In the E-plane, the patterns exhibit a bidirectional tendency, indicating effective radiation characteristics. This comprehensive analysis underscores the antenna's capability to achieve extensive and uniform coverage, crucial for UWB system operations.

Within the passband, the antenna's gain stabilizes at 5 dB. As expected, a decrease in both gain and efficiency is evident within the stopband. These simulations highlight the potential to achieve superior antenna performance in practical applications, especially when utilizing a low-loss substrate during the design phase, thereby enhancing the antenna's efficacy for UWB applications.

Table 2 showcases a comparison of performance metrics between our proposed method and existing filters. Notably, the emphasized values indicate that our approach surpasses others in the field by securing higher S_{11}.

It is imperative to highlight that optimal stopband performance for the parasitic circular patch is attained when the radius is adjusted between $\lambda_g/100$ and $\lambda_g/50$.

TABLE 2. Comparison of performance metrics between different antenna designs

Reference	Size	S_{11}	Notch Band (GHz)	Peak Gain (dB)	Substrate Material
[16]	$0.40\lambda_g \times 1.40\lambda_g$	20 dB	3.3–3.6	10	F4B-M
[17]	$0.59\lambda_g \times 0.54\lambda_g$	25 dB	5.1–5.95	5	FR-4
[18]	$0.26\lambda_g \times 0.19\lambda_g$	20 dB	4.32–5.96	4.8	FR-4
[19]	$0.70\lambda_g \times 0.80\lambda_g$	30 dB	5–6.1	11	TLX-9
[20]	$0.19\lambda_g \times 0.13\lambda_g$	23 dB	5–5.6	4	FR-4
[21]	$0.32\lambda_g \times 0.42\lambda_g$	33 dB	5.2–5.7	5.9	FR-4
[22]	$0.34\lambda_g \times 0.34\lambda_g$	30 dB	3.76–5.90	5	FR-4
[23]	$0.11\lambda_g \times 0.19\lambda_g$	45 dB	4.59–5.82	4.93	RT5880
This work	$0.17\lambda_g \times 0.17\lambda_g$	43 dB	5.43–7.1	5	FR-4

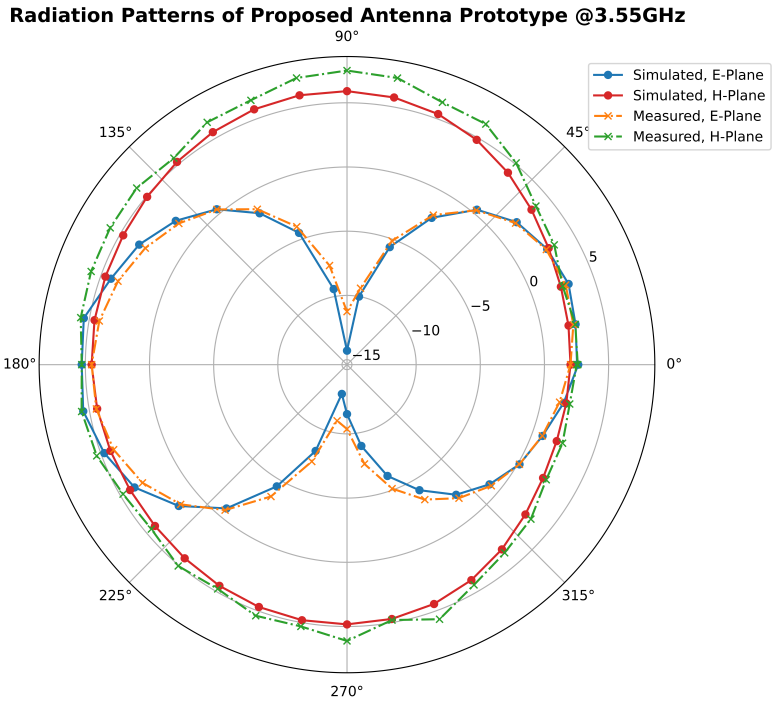

FIGURE 10. Simulated & measured radiation patterns of the proposed antenna prototype.

Moreover, the analysis indicates that variations in the stopband have minimal impact on the antenna's performance within its operational bandwidth, thereby ensuring consistent radiation efficacy. This attribute of the antenna significantly mitigates the challenge of frequency shift, a critical consideration when integrating the antenna into portable devices as an internal component. This capability addresses a pivotal issue associated with frequency displacement, facilitating the antenna's integration into compact electronic devices without compromising performance.

Our current single element design represents the first step towards developing a comprehensive antenna system. We plan to translate this single element model into linear or planar array configurations. When upscaled to an array of antennas, we anticipate improved performance parameters due to the combined effects of multiple elements. The array design will benefit from better material utilization, optimized element separation, and mutual coupling effects, leading to enhanced notch performance and overall antenna characteristics.

4. CONCLUSION

In conclusion, the design and implementation of the UWB antenna with an integrated parasitic circular patch represent a significant advancement in wireless communication technology, backed by careful optimization and rigorous analysis. The antenna achieves a notable return loss of -43 dB at 3.55 GHz, effectively mitigating frequencies from 5.43 to 7.1 GHz with pronounced notching. This capability underscores its practi-

cal applicability in UWB systems, addressing the challenge of unwanted frequency bands with precision. Through careful parameter tuning and simulation using HFSS software, the antenna maintains an omnidirectional radiation pattern and achieves a desirable gain, essential for compatibility across various UWB-enabled devices.

Experimental validation further substantiates the antenna's superior performance, reinforcing its potential for diverse wireless communication applications. Moreover, the integration of the parasitic circular patch enhances the antenna's spectral purity, contributing to its efficiency and functionality in practical scenarios. This design not only offers a cost-effective solution for manufacturing but also meets rigorous industry standards, positioning it as a promising candidate for future wireless communication technologies.

Importantly, simulated results have been carefully matched with measured ones in all aspects, validating the accuracy and reliability of the antenna design. As research and development continue to refine this antenna design, the focus will be on adapting it to evolving industry needs, ensuring its continued growth and integration into the expanding landscape of wireless communications.

ACKNOWLEDGEMENT

The authors would like to thank Dr. Ganga Prasad Pandey and Dr. Vivek Pandit from the Information and Communication Technology, School of Technology, Pandit Deendayal Energy University (PDEU) for their valuable support with measurements.

REFERENCES

[1] FCC, "FCC first report and order on ultra-wideband technology," 2002.

[2] Al-Bawri, S. S., H. H. Goh, M. S. Islam, H. Y. Wong, M. F. Jamlos, A. Narbudowicz, M. Jusoh, T. Sabapathy, R. Khan, and M. T. Islam, "Compact ultra-wideband monopole antenna loaded with metamaterial," *Sensors*, Vol. 20, No. 3, 796, 2020.

[3] Martínez-Lozano, A., C. Blanco-Angulo, H. Garcia-Martínez, R. Gutierrez-Mazon, G. Torregrosa-Penalva, E. A. Navarro, and J. Sabater-Navarro, "UWB-printed rectangular-based monopole antenna for biological tissue analysis," *Electronics*, Vol. 10, No. 3, 304, 2021.

[4] Ramanujam, P., P. G. R. Venkatesan, C. Arumugam, and M. Ponnusamy, "Design of miniaturized super wideband printed monopole antenna operating from 0.7 to 18.5 GHz," *AEU — International Journal of Electronics and Communications*, Vol. 123, 153273, 2020.

[5] Zaidi, A., E. M. Ali, A. G. Alharbi, S. U. Khan, M. Alsharef, M. S. Alzaidi, and S. S. M. Ghoneim, "Multi-mode frequency reconfigurable conformal antenna for modern electronic systems," *Computers, Materials and Continua*, Vol. 73, 3861–3877, 2022.

[6] Awan, W. A., A. Zaidi, M. Hussain, N. Hussain, and I. Syed, "The design of a wideband antenna with notching characteristics for small devices using a genetic algorithm," *Mathematics*, Vol. 9, No. 17, 2113, 2021.

[7] Labiod, M., Z. Mahdjoub, and M. Debab, "Frequency reconfigurable circular microstrip patch antenna with slots for cognitive radio," *TELKOMNIKA (Telecommunication Computing Electronics and Control)*, Vol. 20, No. 4, 740–752, 2022.

[8] Ghaffar, A., X. J. Li, W. A. Awan, and N. Hussain, "Reconfigurable antenna: Analysis and applications," *Wideband, Multiband, and Smart Antenna Systems*, 269–323, 2021.

[9] Iqbal, A., A. Smida, N. K. Mallat, R. Ghayoula, I. Elfergani, J. Rodriguez, and S. Kim, "Frequency and pattern reconfigurable antenna for emerging wireless communication systems," *Electronics*, Vol. 8, No. 4, 407, 2019.

[10] Nazeri, A. H., A. Falahati, and R. M. Edwards, "A novel compact fractal UWB antenna with triple reconfigurable notch reject bands applications," *AEU — International Journal of Electronics and Communications*, Vol. 101, 1–8, 2019.

[11] Li, Y., W. Li, and R. Mittra, "A CPW-fed wide-slot antenna with reconfigurable notch bands for UWB and multi-band communication applications," *Microwave and Optical Technology Letters*, Vol. 55, No. 11, 2777–2782, 2013.

[12] Balanis, C. A., *Antenna Theory: Analysis and Design*, John Wiley & Sons, 2016.

[13] Malik, J., A. Patnaik, and M. V. Kartikeyan, *Compact Antennas for High Data Rate Communication: Ultra-Wideband (UWB) and Multiple-Input-Multiple-Output (MIMO) Technology*, Springer, 2018.

[14] Awan, W. A., A. Zaidi, N. Hussain, A. Iqbal, and A. Baghdad, "Stub loaded, low profile UWB antenna with independently controllable notch-bands," *Microwave and Optical Technology Letters*, Vol. 61, No. 11, 2447–2454, 2019.

[15] Devi, R. and D. K. Neog, "Determination of slot parameters of band-notched ultra wideband antenna using clonal selection algorithm," in *2014 International Conference on Computational Intelligence and Communication Networks*, 60–63, Bhopal, India, 2014.

[16] Xu, L.-J., J. Zhang, Z. Duan, F. Huang, and Y. Li, "Directly connected linear antenna array with band notch characteristics for UWB applications," *IEEE Antennas and Wireless Propagation Letters*, Vol. 22, No. 11, 2685–2689, 2023.

[17] Azim, R. and M. T. Islam, "Compact planar UWB antenna with band notch characteristics for WLAN and DSRC," *Progress In Electromagnetics Research*, Vol. 133, 391–406, 2013.

[18] Zhang, C., Z. Zhao, P. Xiao, J. Yu, Z. Liu, and G. Li, "A miniaturized microstrip antenna with tunable double band-notched characteristics for UWB applications," *Scientific Reports*, Vol. 12, No. 1, 19703, 2022.

[19] Taha-Ahmed, B. and E. M. Lasa, "Polarization diversity UWB antennas with and without notched bands," *Progress In Electromagnetics Research M*, Vol. 76, 101–111, 2018.

[20] Kumar, P., M. P. MM, P. Kumar, T. Ali, M. G. N. Alsath, and V. Suresh, "Characteristics mode analysis-inspired compact UWB antenna with WLAN and X-band notch features for wireless applications," *Journal of Sensor and Actuator Networks*, Vol. 12, No. 3, 37, 2023.

[21] Kumar, O. P., T. Ali, P. Kumar, P. Kumar, and J. Anguera, "An elliptical-shaped dual-band UWB notch antenna for wireless applications," *Applied Sciences*, Vol. 13, No. 3, 1310, 2023.

[22] Rao, P. S., B. S. H. Prasad, J. Kavitha, and U. Jayaram, "A multislot UWB monopole antenna with dual band notch characteristics," *Progress In Electromagnetics Research C*, Vol. 138, 79–90, 2023.

[23] Rizvi, S. N. R., W. A. Awan, D. Choi, N. Hussain, S. G. Park, and N. Kim, "A compact size antenna for extended UWB with WLAN notch band stub," *Applied Sciences*, Vol. 13, No. 7, 4271, 2023.